OPTICAL EMISSION SPECTROSCOPY INVESTIGATION OF A 1-ATM DC GLOW DISCHARGE WITH LIQUID ANODE AND ASSOCIATED SELF-ORGANIZATION PATTERNS

Yao E. Kovach[1], Maria C. Garcia[2,*], John E. Foster[1]

[1]Department of Nuclear Engineering and Radiological Sciences, University of Michigan, Ann Arbor, Michigan, 48109, USA

[2]Department of Applied Physics, University of Cordoba, Ed- C2, Campus de Rabanales, Córdoba, 14071, Spain

*Author for correspondence, e-mail: fa1gamam@uco.es

Abstract

Optical emission spectroscopy is used to study a 1-atm dc helium glow discharge with a liquid anode to obtain insight into the physical mechanisms underlying observed plasma self-organization at the liquid surface. Plasma column conditions such as gas temperature, electron density, and species composition were determined by means of optical emissions spectroscopy techniques and correlated with the appearance and structure of anode patterns over a broad burning voltage range with fixed flow rate and liquid conductivity. The discharge column was stratified from a species standpoint with the attachment near the liquid surface containing more sodium and water emission, while near the cathode, the predominant emission was from nitrogen and helium. The experiment suggested a complex interplay between the transport of liquid phase species and the actual composition of the plasma, suggesting the importance of processes such as localized boiling and perhaps physical sputtering.

Index terms: atomic emission spectroscopy, electrode pattern, non-equilibrium plasma, plasma-electrode interaction, plasma on liquid, plasma spectroscopy.

I.   Introduction

Self-organization is ubiquitous in nature [1]. In general, it tends to result from competing effects and may be considered a consequence of an instability or a multivalued equilibrium solution. In low-temperature plasma physics, self-organization of anode spots into distinct patterns that are either static or in motion has been observed for some time dating back to the 1900s [2]. These patterns have been observed in high-pressure discharges with both liquid and solid electrodes. In such discharges, the attachment at the anode is observed to transition from a uniform discharge spot at the anode to highly structured patterns that are either static or in motion. The theoretical basis for the spot formation has advanced in recent years with computational models actually replicating the self-organization at least in 2- D models. In this regard, no "new" physics is required to replicate their appearance computationally. Theoretically, reaction–diffusion models have been used with limited success in at least qualitatively explaining observed self-organization phenomena [3]. Here, self-organization results from competing effects where there are an activator and an inhibitor. For example, the competition between the current density—the activator and the anode fall voltage—the inhibitor can give rise to spot phenomena [4], [5]. Here, the anode voltage variations can drive stratification of the attachment at the anode ultimately leading to separation into spots. Local space charge also plays a key role in self-organization. In this case, the competition is between the space charge and the diffusion [6], [7]. Some of the theory of anode spot self-organization suggests the need for a resistive anode or ohmic barrier at the anode surface. The ohmic barrier would tend to regulate and thus stabilize the current flow and the resulting pattern [3], [8]. However, self-organization of anode spots has been experimentally observed also on bare anodes, which shows that the presence of a resistive anode is not a decisive

condition for self-organization. Raizer and Mokrov [9] suggest that space charge can give rise to filamentation and thus the redistribution of the electric field at the surface, which can lead to self-organization. Muller [8] suggests that pattern formation is a consequence of a bistable layer in contact with a resistive zone at the anode surface. The bistable layer is modeled as an S-shaped current–voltage characteristic. Here, the formalism is again the reaction–diffusion equation. Metastable solutions associated with the local minima in a generalized potential are associated with the observed anode patterns. Muller also asserts that Coulombic effects determine spot behavior on the surface. Anode spots tend to interact repulsively. The spatial distribution of plasma structures on the surface of the electrode, whether liquid or metal should therefore tend to form a pattern that minimizes the energy of the system. Berezin [10] was able to show that the minimum energy configuration of localized charges at such spots were not necessarily always corresponded to all the attachments that located at the circumference, but rather above a certain spot number, subsequent attachments placed in the center with minimized energy. Such interactions invariably determine pattern spatial distribution. Muller used a generalized potential term associated with Coulombic interactions between plasma attachments to account for repulsion effects. Trelles [11] using a time-dependent nonequilibrium model was able to show the formation of anode spots in a high-current free-burning arc discharge. The self-organization observed in this case is similar to the anode patterns observed in atmospheric pressure glows. This model suggests that anode cooling plays a key role in self-organization. The model suggests that heavy particle cooling at the anode, which lowers heavy particle temperature impacts plasma conductivity and ultimately electron collection at anode. To maintain equilibrium, electron temperature must increase to maintain plasma conductivity. No chemical or electrode effects were included in model yet it reproduced the spot patterns observed experimentally, thus highlighting the cooling effect. Trelles

goes on to suggest that the anode spot patterns represent multiple possible solutions, which can lead to steady state. Recently, Bieniek et al. [12] have shown by numerical modeling that the self-organization does not fit into the conventional pattern of self-organization in bistable nonlinear dissipative systems. This modeling has revealed a connection between the self-organization and the reversal of the near-anode potential drop. Experimental insight, however, has lagged theory. Although there is some framework for the theoretical basis for spot formation, it is, in general, difficult to measure the experimental parameters that would facilitate either model validation or suggest additional model development [13]. Experiments carried out to date, however, have elucidated key variables governing spot formation. For example, Verreycken [14] showed that for atmospheric pressure glows on liquid anodes, spot number increases in input current and tends to decrease with liquid conductivity. They also confirmed with high-speed imaging that the spot patterns observed are not a consequence of a single fast-moving attachment. Pattern rotation was attributed to negative ions in [14]. Wilson et al. [15] also attributed the rotation of a ring-shaped attachment on a liquid anode to negative ion production. In this work, rotation was found to occur in air but not in pure nitrogen, hydrogen, or helium environments. This study did not find a correlation between cathode material and pattern behavior, suggesting that the effect is largely local, independent of cathode electrode processes. Bruggeman et al. [16] used high-speed imaging to generate spatial maps of the discharge attachment with a liquid anode and found its structure was similar to that of a typical glow discharge [16]. In this experiment, the gas flow was not injected through the cathode, but rather the glow was generated in a pressure vessel operating at roughly 1 atm in which the background gas composition could be varied. The gas temperature of the column was estimated from emission spectra measurements to be ~3000 K. The temperature near the anode surface was considerably lower. This cooling is due to the liquid water acting as a heat sink. This

temperature drop was suggested as the mechanism for stabilizing the discharge via cooling in addition to acting as a resistive layer to current flow. This observation is consistent with Trelles's simulations, which purported of the importance of cooling of the anode region of a free-burning arc [11]. It should also be pointed out that Bruggeman and colleagues observed an increase in OH emission near the anode. This was attributed to higher water vapor concentration there [16]. Shirai [17]–[19] have also carried out extensive anode pattern studies on both liquid and solid electrodes. They also observed dependence of the anode spot pattern on gas composition. They found that spots did not appear in predominantly helium and water vapor environments [18]. Furthermore, they noted that injected oxygen had a strong effect on the self-organization pattern, thereby suggesting the action of gas-phase chemical reactions and the production of negative ions [17]. Indeed, spot formation tended to take place in those regions where oxygen was injected. They also observed that the plasma-induced emission in the plasma column of the glow did not differ appreciably from the anode attachment. A liquid anode temperature dependence was also noted. Here, they found that anode spot patterns became more complex when the liquid temperature was actively raised. This effect was attributed in part to the influence of water vapor [17]. They observed a polarity dependence in the point to plane geometry studied. When the cathode was configured as the liquid electrode, cathode spot patterns did not appear on the liquid surface [17]. Miao et al. [20] investigated a conical attachment on a liquid anode. This work reported on the fluid dynamical effects driven at the anode surface by the anode attachment such as ripples. This work suggested the key role of surface charging, which may stabilize the discharge at low water conductivities. At higher conductivities, it was found that the discharge tended to be unstable. As can be seen from this survey of anode pattern formation in atmospheric pressure glow studies, competing processes such as diffusion and space charge in the presence of a resistive

conducting electrode play important roles in discharge surface attachment behavior. A requirement of any self-organization process is that the system is driven far from thermal equilibrium and that in the presence of random fluctuations in the presence of feedback, the organization process is amplified [21]. Such local negative entropy changes, which give rise to organization are possible in open systems where there is nonlinear dissipation. The dissipated energy exits the system globally so that the entropy increases globally but reactants are constantly being replenished in this case from the plasma. In general, such self-organization arising from reaction–diffusion systems is derived in some manner from a balance between a local activator (for example current) and the inhibitor (diffusion/voltage) [22], [23]. The key to understanding the self-organization process is the identification and subsequent quantification of these parameters. What adds to the complexity of the dc atmospheric glow with liquid anode is that during the operation, the solution itself chemically changes leading to temporal and spatial variations in conductivity, pH, and concentration. These, in turn, can lead spatially varying reaction-diffusion systems, which, in turn, can seed plasma pattern formation as well. From the experimental data, it is clear that the spot formation is a local process with a strong dependence on gas composition and surface conductivity. In this work, we investigate the general structure of the atmospheric pressure glow spectroscopically. Here, variation in species and discharge temperature along the plasma column is ascertained along with the plasma density. The localized attachment at the liquid surface is the source of input water vapor. Such localized boiling is also a source of droplets, which also contains ions in the electrolytic solution. The presence of this gas source influences ionization rates and energy transfer in the plasma column and is also a source of feedback, that is, the higher the current, the higher the evaporation rate. This interchange may play a role in the formation of the self-organization patterns on the surface. In this work, we investigate

the influence of water vapor and in-solution ions on discharge characteristics as a function of operating condition using optical emission spectroscopy (OES) techniques as well and correlate these changes with observed changes in the self-organization pattern at the liquid surface.

II. Experimental Setup

Fig. 1 shows a schematic of the discharge apparatus, which is of the point to plane geometry. The cathode is a 6-mm-diameter brass rod, with a 500-μm orifice through which helium, the working gas, is expelled at a nominal flow rate of 200 standard cubic centimeters per minute (SCCM). The discharge itself operated in regular room air. The cathode was connected to a dc power supply (Gamma High Voltage Research) with 0–3-kV and 0–400-mA voltage and current ranges, respectively. This arrangement is in contrast with the Verreycken study [14], in which the discharge develops along a jet of flowing helium. The liquid anode consisted of a NaCl solution with an initial concentration of 9 g/L and an initial electric conductivity of 12 mS·cm−1 at room temperature in contact with a grounded return electrode [19]. The distance between the cathode and the liquid was adjustable using a computer-controlled stepper motor-based motion control system. The interelectrode spacing could be varied between 1 and 8 mm. The schematic depiction of the apparatus along with an actual discharge attachment at the liquid anode surface is shown in Fig. 1.
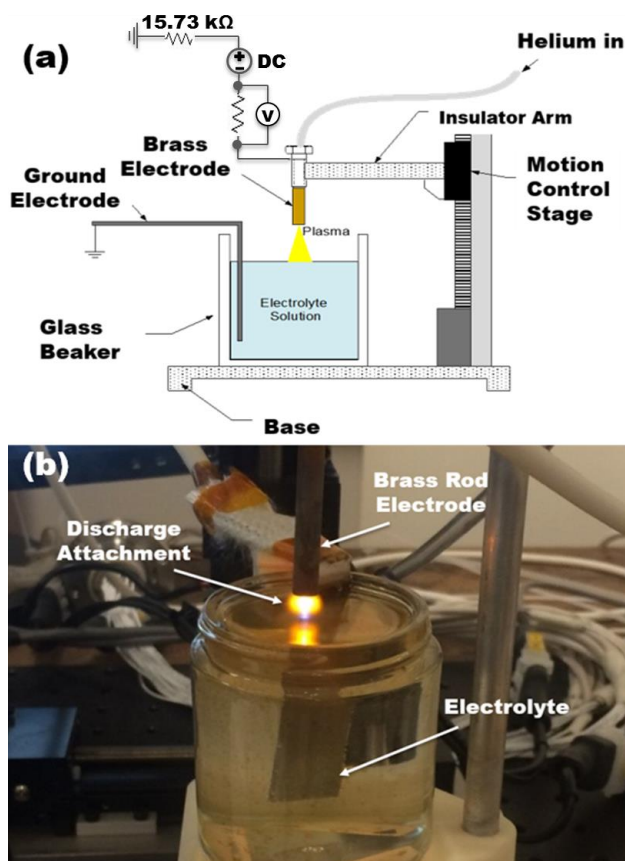
Figure 1. Experimental setup is shown in (a) sketch of the discharge configuration (not to scale) with a photo of (b) operation in 1 atm DC glow.

For a given spectroscopic measurement, the current and voltage were constant. Depending on the current, voltage, and interelectrode gap, different plasma emission patterns were observed on the liquid surface. As shown in Fig. 1, for every voltage condition, the discharge current was determined from the voltage drop across a 100-Ω resistor, which connected in series with the 15.73- kΩ resistor. Pictures of the emission patterns of the discharge were obtained using a charge-coupled device (CCD) camera with sensitivity in the UV and visible regions. OES techniques were employed to diagnose plasma generated over the liquid. Fig. 2 schematically depicts the experimental setup used to acquire the OES measurements. Light emission from the plasma was analyzed by using a Czerny– Turner type spectrometer (Acton Series, SP-2300i) of 0.3-m focal length equipped with an 1800-grooves/mm holographic grating, and a fast

intensified CCD camera (PI-MAX3, Prince ton Instruments) was used as a detector. The spectra were recorded with a spectral resolution (measured through the instrumental broadening) of 0.13 nm.
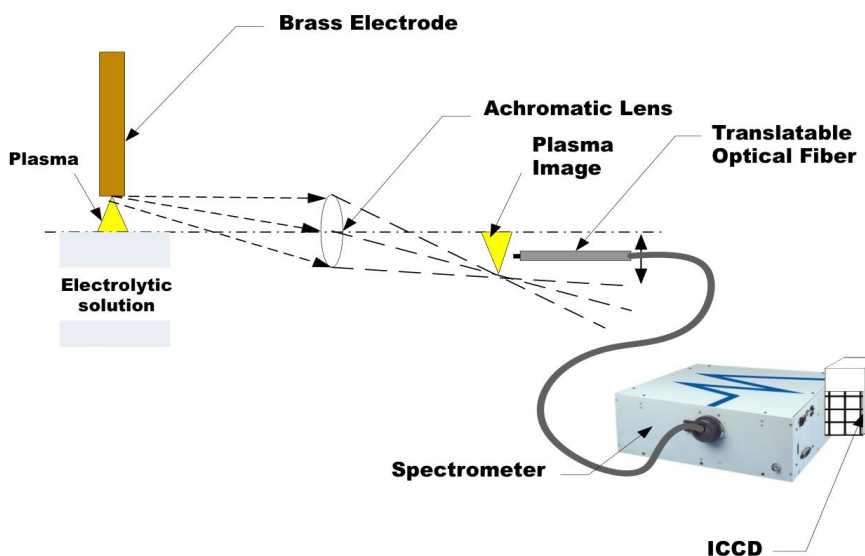

Figure 2. Schematic depiction of imaging approach for OES diagnostic

Line-integrated emission spectra acquired at different axial positions along the axis of the plasma column relative to the position of the cathode exit plane (z = 0, 3, 5, and 8 mm) were collected and focused at 1:1 magnification onto an optical fiber using an achromatic lens. Position z = 8 mm corresponded to the discharge position at the liquid anode surface. For each experimental condition, the spectrum was recorded three times. In order to deal with water evaporation and keep the distance constant, the beaker was refilled with water until a mark and refilled after every single measurement. The spatially resolved emission spectra were used to determine the spatial variations in species, gas temperature, excitation temperature, and electron density along the discharge axis.

III. Results

A. Self-organization patterns and V-I character

The discharge attachment at the surface of the anode varied with the applied voltage. In this work, the discharge gap was fixed at 8 mm from the end face of the powered electrode to the surface of the water. Fig. 3 illustrates the variations in the discharge current with the voltage applied across the gap. Discharge voltage and associated discharge current are summarized in Table I, which includes the total voltage applied as well as the gap voltage, the total voltage minus the series resistance voltage drop.
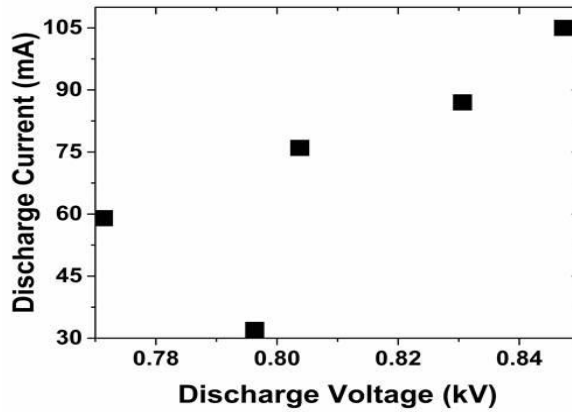

Figure 3. Discharge current variations with discharge voltage

Table I. Voltage and current values in the plasma.

Total Voltage V(kV)	Gap Discharge Voltage (kV)	I (mA)
1.3	0.796	32
1.7	0.771	59
2.0	0.804	76
2.2	0.831	87
2.5	0.848	105

As can be seen in the figure, generally, the discharge current increases with increasing applied voltage. Above an applied voltage of 1.3 kV, the discharge impedance drops.

With increasing applied voltage, gap impedance decreases by nearly a factor of two. The appearance of a spoke like attachment accompanies the initial drop in impedance, suggesting that the pattern is essentially a preferred, lower resistance pathway toward discharge maintenance, in contrast to the double ring attachment. Interestingly, over the range of total applied voltages, the gap voltage is relatively constant ~0.8 kV, which is behavior typical of a normal glow. In a normal glow, the discharge is sustained by secondary electron emission. The case of the 1-atm glow with the liquid anode, vaporization of water and metal ions derived from droplets associated with localized boiling at the attachment may be the secondary process that plays a role in sustaining the anode spots. Under these experimental conditions with the exception of the lowest burning voltage, self-organization patterns were observed on the surface of the water. Fig. 4(a)–(e) shows the spatial optical emission patterns observed for different voltage (current) conditions listed in Table I.
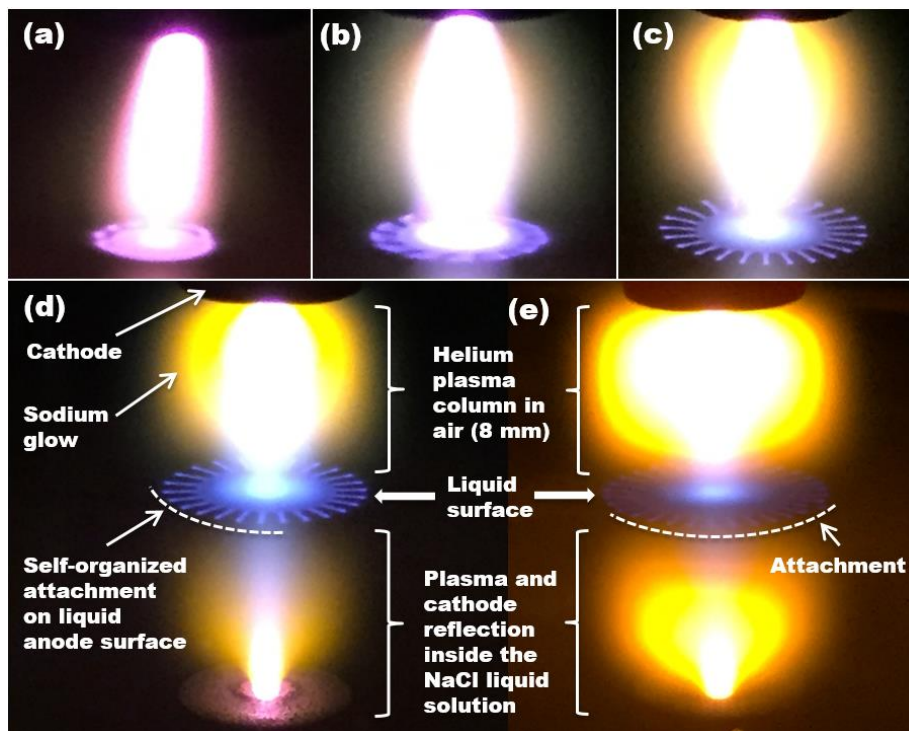

Figure 4. Variation in discharge column and attachment shape with increasing the total voltage: (a) V = 1.3 kV; (b) V = 1.7 kV; (c) V = 2.0 kV; (d) V = 2.2 kV and, (e) V = 2.5 kV.

For total applied voltage of V = 1.3 kV [Fig. 4(a)], a ringlike pattern was observed. Three apparent changes were observed to occur with increasing voltage. The attachment at the anode attachment structure differentiated into a well-defined wagon wheellike pattern with increasing voltage with the spoke length and number increasing with increasing voltage. This observation is similar to Shirai et al. [24] where the wagon wheel and gearlike structures were observed at the higher currents corresponding to elevated voltages. Fig. 5 illustrates the variation in spoke number with gap voltage. As can be seen here, initially, at breakdown and subsequent discharge formation, there are no spokes at all. Subsequent increase in the discharge current gives rise to the formation of spokes as well as an initial small decrease in discharge voltage. Apparently, spokes occur only above a threshold discharge current. Once the pattern has formed, the number of spokes tends to increase monotonically with increasing discharge current as can be seen in the figure. The anode attachment at the surface became bluer with increasing voltage as well, which could indicate a change in the local electric field reflecting changes in the nature of dissipation there (e.g., electron heating, increased collisionality). The shape of the discharge column was also observed to change with increasing voltage, changing from cylindrical to oblong to an oblate spheroid cloud. The color of the discharge attachment changed with increasing voltage as well, transitioning from purple pink to yellow, indicating the intrusion of sodium into the discharge. The mechanism for sodium transport is not well understood though localized boiling likely plays a key role. It is well known that fine droplets leave with the steam [25]. Indeed, in industrial applications, such droplets are problematic in that it leads to the deposition of corrosive deposits such as salts in steam generation systems and boilers [25], [26]. The evaporation of these fine droplets in the gas state is a likely source of sodium in the gas phase. Indeed,

Shirai and colleagues have observed the presence of electrolyte species in the gas phase for a dc glow with the liquid cathode. Droplet evolution may play some role in these observations as alluded to in that work as well [27]. Field-induced extraction is possible as well if the local field in the sheath is high enough. Also, associated with high localized fields is Taylor cone formation, which can produce jets of fine droplets injected into the gas phase [13]. As will be discussed later, the presence of this cloud is accompanied with a reduction of the plasma emission from positions z = 3 mm and z = 5 mm along the axis. As can be inferred from the reflection images, the sodium cloud appears to extend to the cathode region of the discharge. The anode spot patterns observed on the surface were not always static, rather in cases, the pattern rotated about its vertical axis of symmetry.
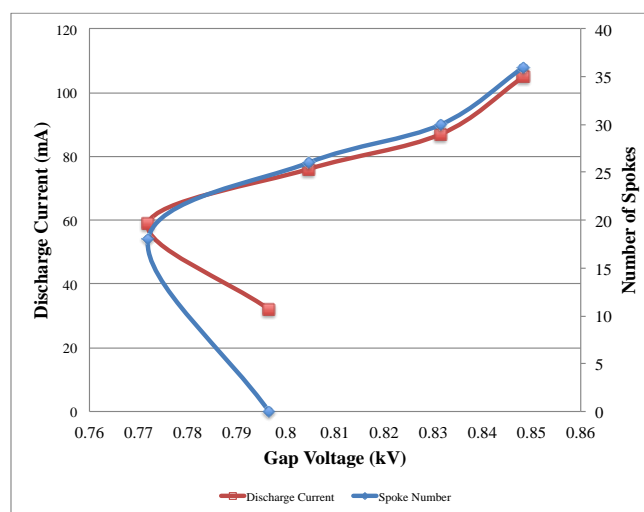

Figure 5. Discharge current and spoke number variation with gap discharge voltage.

B. Optical Emission Spectra

Fig. 6(a)–(c) shows typical optical spectra emitted from 300 to 800 nm at different axial positions: (a) exit plane of the cathode; (b) midpoint of the plasma column; and (c) just above the liquid surface.

13

In all cases, the most prominent peaks correspond to the OH emission (3060 Å system). A strong emission was also detected for NH (3360 Å) and N2 (second positive) systems, especially under lower voltage conditions (1.3 kV). For higher voltages, the emission of N2 (second positive) notably reduced. Weak emissions of He I lines and atomic hydrogen Balmer series lines (Hα and Hβ) are observed. Fe I lines (368.74 nm, 406.36 nm, with upper level energies of 4.2 and 4.6 eV, respectively) were also identified in the spectra at 2.5 kV. The presence of iron is most likely due to the evaporation of solvated iron ions in solution. The iron ion source in solution is presumably the immersed return electrode. The iron electrode supplies ions into the solution. These ions are reduced in the plasma attachment and evaporate as iron. Shirai et al. [28] used an iron anode to serve as an iron ion source for the production of ferrous nanoparticles in solution. Na I 589.0 and 589.6 nm lines, corresponding to resonant transitions from 3p states of sodium atomic system (of very low excitation energy, 2.1 eV) toward the ground state, were also detected. The presence of sodium is also attributed to the evaporation of solvated sodium ions. These lines were most intense in the mid region rather than near the liquid surface where presumably the sodium concentration is highest. The contradiction is resolved if the electron temperature near the surface is simply too cool (owing the high evaporation rates there) to support a sufficiently high excitation rate. Direct measurements of temperature using a collisional–radiative model would be required to fully understand electron dynamics at the surface, which is left to future work.
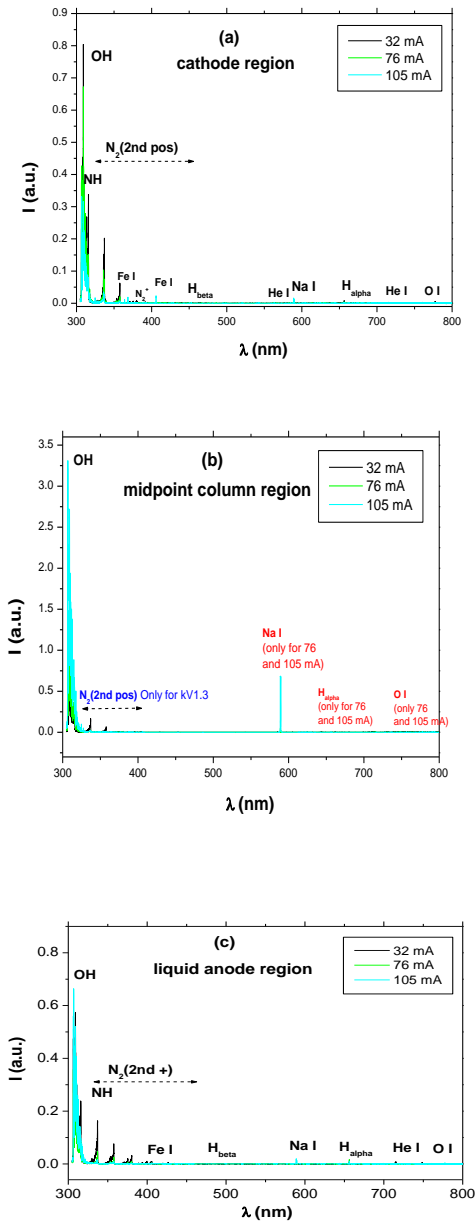
Figure 6. Emission spectra along plasma column: (a) Cathode region (z = 0 mm); (b) midpoint column region (z = 3 mm); (c) liquid anode region (z = 8 mm).

1) Vapor Cloud Optical Emission: Interestingly, the mid region of the plasma discharge is bulb shaped at elevated voltages and is yellow in color—owing to the presence of sodium. The shape of the cloud can be explained if one assumes that the discharge attachment is highly localized. This assumption is consistent with the relatively small diameter of the self-organized patterns < 1 mm, corresponding to current densities approaching 20 A/cm^2. The localized attachment gives rise to localized boiling and droplet entrainment with steam. Evaporation and droplet evolution, in this case, take the form of a cosine distribution [29]. If the steam and droplet evolution rate is relatively high, then the evolved water tends to be focused with the shape of the plume following a modified cosine distribution scaling as $\sim(\cos\phi)^n$, where ϕ is the angle relative to the surface normal. In such a case, the nature of the evaporated plume depends on the ratio of the heat source size to the equivalent mean free path of the evaporating particle, n [30]. The uncertainty in this work is the actual temperature of the water at the attachment, which could range from 373 K to temperatures approaching the spectroscopically determined gas phase just above the liquid surface of $\sim$1000 K. Over such a temperature range, the local vapor pressure as determined by the Clasius–Clapeyron equation can vary by many orders of magnitude greatly exceeding the local atmospheric pressure. Associated with such high local pressures is the neutral flux, which scales linearly with vapor pressure, leading to focused emission and an asymptotic value of approximately 3 for n. Interestingly, such focusing effects are affected by the nature of the attachment. Here, self-organization can actually seed the nature of the vapor plume. Electron diffusion from the main column excites the water vapor and sodium vapor (produced from evaporating droplets), giving rise to the sodium cloud glow as observed in the experiment. This situation is depicted schematically in Fig. 7. The excitation threshold of the sodium D lines is low $\sim$2 eV. Hot electrons as they diffuse radially outward, losing energy along the way from the core to

the terminal radius where they can still excite the sodium. The reduced nitrogen intensity at the higher voltage may also be a manifestation of electron cooling via collisions with water molecules, whose flux into the gas phase increases with the input voltage. In summary, the observation of metal ions in the gas phase is notable in that it highlights a transport mechanism for solute atoms or molecules in solution driven by the plasma. Such transport also acts as a feedback mechanism, impacting overall plasma column impedance. The relative importance of water injection into the discharge can be estimated. The ratio of water vapor evaporation to helium flow rate yields the relative importance of various gases to discharge maintenance. The evaporation flux from the located plasma attachment at the liquid surface is related to the local vapor pressure, p_v:

$\Gamma = \frac{p_v}{\sqrt{3\pi m k T}}$, where m is the water molecule mass, k is Boltzmann's constant, and T is the temperature of the water at the attachment. The ratio of water molecules emitted from a square millimeter area to the number per unit time of injected helium molecules is approximately 10. Indeed, the discharge is indeed dominated by the water vapor evaporation.
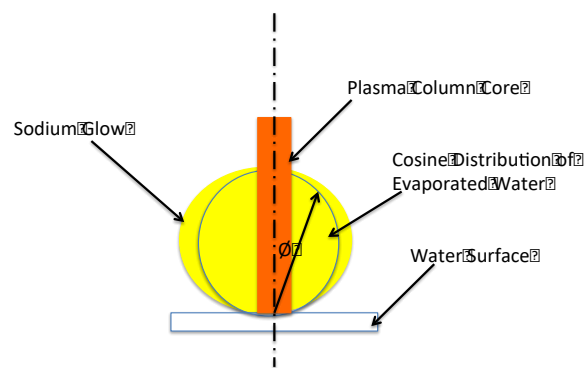

Figure 7. Possible mechanism for the bulb shaped sodium cloud.

2) Excited Species in Plasma Column: Table II summarizes plasma excited species observed in the emission spectra (marked with "x") as a function of current. The NH radical was also detected suggesting plasma-activated chemistry between ambient nitrogen and water vapor derived from the anode. This multistep process can lead to the formation of NH. It was only observed near the cathode suggesting that its production requires energetic electrons. The production of NH in similar plasmas has been studied. Here, two mechanisms are possible. In one case, if the nitrogen is sufficiently energetic (~1 eV) then: $N+H_2 \rightarrow NH+H$. Activation energy for such a reaction is high. Although near the cathode, the plasma temperatures can reach several thousand kelvin, it is unlikely that this mechanism dominates but perhaps contributes at a lower production rate. The following reaction is also plausible: $N^++H_2 \rightarrow NH+H^+$ [31]. Emission from the axis of the discharge at middle positions was greatly reduced at the high voltage, higher current conditions. The density of the vapor cloud is expected to increase with increasing voltage since the discharge current and thus power deposited into the liquid also increase. The cloud presumably consists of sodium, helium, and water vapor. The origin of this reduced emission (at levels below the detection sensitivity of the optical system) could be ascribed to both, the very low electron temperature values in these cases (as shown later) and also to the quenching of excited states provoked by the presence of water vapor [32]. Alternatively, at elevated power, the vapor cloud may serve as a resistive barrier to electron transport. The supersaturated vapor region in the vicinity of the attachment would reduce electron mobil ity (E/N reduced), reduce electron temperature, and increase locally electron losses by attachment. This obstructed flow could possibly contribute in part to the visible shape of the positive column. Electron density and flow would tend to be higher along the outer surface of the vapor cloud where the E/N is higher and collisionality reduced. This effect would also contribute to pattern formation as electron flow is no longer strictly axial. Evidence

supporting this vapor barrier mechanism comes from observed water evaporation rates. In general, for the 200-mL jars used in this experiment, the water level was observed to drop at an average rate in the order of 0.15 mm/min due to evaporation. Evaporation occurs at the localized plasma attachment point as the bulk solution was under the boiling temperature. This 0.15-mm/min level drop corresponds to a water evaporation rate of about upto 1 SCCM of water vapor into the discharge, saturating the volume above the surface with water vapor including likely water clusters as well. It is this upward rising neutral gas that has the potential to cool the plasma near the liquid surface thereby reducing excitation by electron impact on that region. This vapor effect is a function of power and may indeed serve as ballasting for the discharge. At high powers, its likely that ionization makeup for losses in the vapor layer must come from ionization processes driven by sheath effects at the liquid surface. Future work will involve absorption spectroscopy to elucicated the role of this water vapor "fountain" effect. Interestingly, the helium emission was found near the surface of the liquid. These emission lines have their upper levels lying around 23 eV suggesting the presence of energetic electrons. The presence of energetic electrons, in turn, suggests the presence of an appreciable voltage drop at the liquid surface. In addition, visually at the liquid surface, the discharge manifests itself as a localized plasma attachment distinct and essentially detached from the main plasma column. This surface plasma is presumably produced by electron impact, implying the presence of an electron accelerating sheath that serves as the energy source. This sheath, therefore, may be the source of energy for the self-organization patterns at the surface, which, in turn, supports the notion that the patterns are a type of anode spot similar in nature to low-pressure variants.

Table II. Spectroscopic features of species observed by OES in the plasma.

Species	λ (nm)	Transition	E_u (eV)	I (32 mA)	I (76 mA)	I (105 mA)	Region of the spectrum
OH	308.90	$A^2\Sigma^+ \rightarrow X^2\Pi$	4.0	x	x	x	UV
NH	336.01	$A^3\Pi \rightarrow X^3\Sigma^-$	3.4	x	x	Only next the cathode	
N_2	315.93	$C^3\Pi_u \rightarrow B^3\Pi_g$	11.1	x	x	Only next the cathode	
	337.13	$C^3\Pi_u \rightarrow B^3\Pi_g$	11.1	x	x		
	353.67	$C^3\Pi_u \rightarrow B^3\Pi_g$	11.1	x			
	357.69	$C^3\Pi_u \rightarrow B^3\Pi_g$	11.1	x	x		
	367.19	$C^3\Pi_u \rightarrow B^3\Pi_g$	11.1	x			
	371.05	$C^3\Pi_u \rightarrow B^3\Pi_g$	11.1	x			
	375.54	$C^3\Pi_u \rightarrow B^3\Pi_g$	11.1	x	x		
	380.49	$C^3\Pi_u \rightarrow B^3\Pi_g$	11.1	x	x	x	
	385.79	$C^3\Pi_u \rightarrow B^3\Pi_g$	11.1	x			Violet
	389.46	$C^3\Pi_u \rightarrow B^3\Pi_g$	11.1	x			
	394.30	$C^3\Pi_u \rightarrow B^3\Pi_g$	11.1	x	x	x	
	399.84	$C^3\Pi_u \rightarrow B^3\Pi_g$	11.1	x	x	x	
	405.94	$C^3\Pi_u \rightarrow B^3\Pi_g$	11.1	x	x		
	409.48	$C^3\Pi_u \rightarrow B^3\Pi_g$	11.1	x			
	414.18	$C^3\Pi_u \rightarrow B^3\Pi_g$	11.1	x			
	420.05	$C^3\Pi_u \rightarrow B^3\Pi_g$	11.1	x			
Fe I	368.74	$4p \rightarrow 4s$	4.2			x	
	406.36	$4p \rightarrow 4s$	4.6			x	
N_2^+	391.44	$B^2\Sigma_u^+ \rightarrow X^2\Sigma_g^+$	18.9	x	x	Only next the cathode	
N_2	426.97	$C^3\Pi_u \rightarrow B^3\Pi_g$	11.1	x	x	Only next the cathode	Indigo
	434.36	$C^3\Pi_u \rightarrow B^3\Pi_g$	11.1	x	x	Only next the cathode	
	441.67	$C^3\Pi_u \rightarrow B^3\Pi_g$	11.1	x			Blue
	449.02	$C^3\Pi_u \rightarrow B^3\Pi_g$	11.1	x			
	457.43	$C^3\Pi_u \rightarrow B^3\Pi_g$	11.1	x			
	481.47	$C^3\Pi_u \rightarrow B^3\Pi_g$	11.1	x			
H I (H_β)	486.13	$4d \rightarrow 2p$	12.7	x	x	x	
He I	501.56	$3p \rightarrow 2s$	23.1	x			Green

	587.56	*3d →2p*	23.1	x	x	Only next the cathode and liquid	Orange
Na I	589.00	*3p → 3s*	2.1		x	x	
	589.60	*3p →3s*	2.1		x	x	
H I (Hα)	656.27	*3d →2p*	12.1	x	x	x	Red
He I	667.81	*3d →2p*	23.1	x	x	Only next the cathode and liquid	
O I	777.19	*3p → 3s*	10.7	x	x	x	
	777.42	*3p → 3s*	10.7	x	x	x	
	777.54	*3p → 3s*	10.7	x	x	x	

C. Gas Temperature

The gas temperature (T_{gas}) was estimated from the rotational temperature deduced from the theoretical simulation of OH(A-X) spectra and their comparisons to the experimental ones. The spectra were simulated using LIFBASE software developed by Luque and Crosley [33], using an instrumental resolution of 0.13 nm. Fig. 8 shows the values of Tgas measured for different discharges studied. Unlike 32-mA case, in which the gas temperature is relatively constant along the axis of the discharge, for the rest of cases, the gas temperature decreased at positions closer to the liquid, suggesting modest cooling at the liquid surface. This is to say that evaporative cooling is more important to discharge at the higher currents. Indeed, the patterns may be comprised predominantly of water vapor plasma. Interestingly, there is a steep gas temperature drop-off beyond the cathode. The temperature in the mid-discharge region and beyond is relatively constant. Here, it is conjectured that the evaporation of water into the discharge regulates the gas temperature. In many respects, it acts to cool the discharge. The combination of this cooling effect and the forced convection owing to the injected helium flow likely plays a key role in stabilizing the discharge as well. Magnitudewise, based on these measurements, the discharge is hot but nonthermal in nature with heavy species

temperature of order a tenth of an electron volt with electron temperatures expected in the range of a few electronvolts [13].
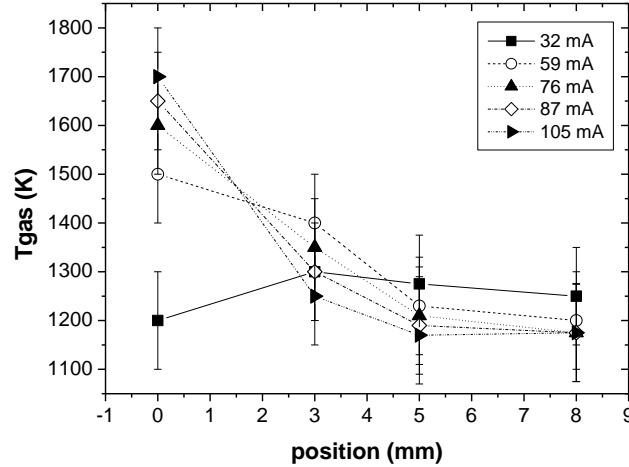

Figure 8. Axial evolution of the gas temperatures for the different plasma columns

D. Electron density

The electron density (n_e) of the discharge was determined from the Stark broadening of H$_\beta$ (486.13 nm) atomic hydrogen Balmer series line. The profile shape of this line is very sensitive to the micro-elecric field induced by charged particles (electrons and ions) that surrounds the emitter atom (H). H$_\beta$ line is commonly employed for determination of electron densities from 10^{20} m^{-3} and above [34]. Even though H$_\alpha$ has a higher intensity, this line is less suitable to measure n_e (especially for small electron densities cases, and optical systems with not very high spectral resolutions) due to its smaller due to its smaller full width at half maximum (FWHM), its higher sensitivity to self-absorption and its stronger dependence on kinetic equilibrium conditions in the plasma.

It was assumed that the profile of the emitted H$_\beta$ line has a Voigt profile, a convolution of a Gaussian shape profile, and a Lorentzian shape profile. The Gaussian

line contribution is attributed to the *Doppler and instrumental* broadening and Lorentzian part is associated with *van der Waals* and *Stark* broadenings. The line full width at half maximum of this Voigt profile $\Delta\lambda_V$ is related to the Lorentzian and Gaussian contributions through the expression:

$$\Delta\lambda_V = \frac{\Delta\lambda_L}{2} + \sqrt{\left(\frac{\Delta\lambda_L}{2}\right)^2 + \Delta\lambda_G^2}$$

(1)

The *van der Waals* broadening contributing to the Lorentzian FWHM of the H$_\beta$ line was calculated using the expression [35]:

$$\Delta\lambda_{vdw} = \frac{C}{T_{gas}^{0.7}} (nm)$$

(2)

The coefficient C in eq. (2) was calculated in first instance for helium as perturbing atom resulting in a value of 2.5, in a similar way to the coefficients obtained by Laux et al. [36] and by Bruggemann et al (2009) [37] for air and water vapor perturbing molecules (3.6 and 4.10, respectively). In these plasmas with relatively low gas temperature, the van der Waals contribution has a non-negligible effect [38].

On the other hand, the Doppler broadening contributing to the Gaussian FWHM of the H$_\beta$ line was calculated from

$$\Delta\lambda_{Doppler} = 3.48 \times 10^{-4} T_{gas}^{1/2} (nm)$$

(3)

The H$_\beta$ line profile detected was also affected by the instrumental function of the spectrometer and experienced an *Instrumental* broadening $\Delta\lambda_I$. The instrumental function of the spectrometer was measured from the profile line Ne I 632.8 nm emitted by a helium-neon laser. When using equal entrance slit width and CCD pixel width, this

function has an approximately triangular shape, well fitted with a Gaussian function [34]. From the FWHM of this line a $\Delta\lambda_I$ = 0.13 nm was measured.

Thus, the Voigt FWHM was measured from the best Voigt profile fit, and taking into account the abovementioned considerations, the actual *Stark* broadening for line was determined. The electron density was derived from $\Delta\lambda_{Stark}$ using the following equation [34]:

$$\Delta\lambda_{Stark} = 4.8 \times \left(\frac{n_e}{10^{23}\, m^{-3}} \right)^{0.68116} (nm)$$

(4)

The H$_\beta$ line could not be detected at positions z = 3 and 5 mm in many cases, thereby precluding calculation of the electron density at these positions. Table III gathers the Voigt FWHM measured for H$_\beta$ line at z = 0 and z = 8 mm positions, $\Delta\lambda_V$. It also includes their corresponding Lorentzian contributions $\Delta\lambda_L$ calculated from them using (1), and taking into account that the Gaussian contribution is given by

$$\Delta\lambda_G^2 = \Delta\lambda_{Doppler}^2 + \Delta\lambda_I^2$$

(5)

The van der Waals contribution was determined from (2) considering both, a 100% of helium and 100% vapor surrounding hydrogen atoms [35]. Finally, their corresponding Stark contributions were determined from the following expression:

$$\Delta\lambda_L = \Delta\lambda_{vdw} + \Delta\lambda_{Stark}$$

(6)

It should be pointed out that the van der Waals contribution to the lorentzian FWHM depends on the type of gas surrounding the emitter atom (hydrogen). This dependence does affect the determination of the Stark contribution and, eventually, the

electron density determination. Changes of $\Delta\lambda_{Stark}$ upon current increases are also presented in Table III.

Table III. Widths for H_β line at z = 0 and z = 8 mm positions.

I (mA)	$\Delta\lambda_V$(nm)	T_{gas} (K)	$\Delta\lambda_L$(nm)	$\Delta\lambda_{VDW}$(nm) (supp 100 % vapor surr H)	$\Delta\lambda_{Stark}$(nm) (supp 100 % vapor in VDW)	$\Delta\lambda_{VDW}$(nm) (supp 100 % He surr H)	$\Delta\lambda_{Stark}$(nm) (100 % He in VDW)
z = 0 mm							
32	0.1640 ± 0.0010	1200 ± 100	0.0601 ± 0.0010	0.0287 ± 0.0017	0.0310 ± 0.0020	0.0177 ± 0.0010	0.0424 ± 0.0014
59	0.1706 ± 0.0001	1500 ± 100	0.0705 ± 0.0006	0.0245 ± 0.0011	0.0460 ± 0.0013	0.0151 ± 0.0007	0.0553 ± 0.0010
76	0.1713 ± 0.0003	1600 ± 100	0.0715 ± 0.0006	0.0234 ± 0.0010	0.0481 ± 0.0012	0.0144 ± 0.0006	0.0570 ± 0.0009
87	0.1733 ± 0.0006	1650 ± 100	0.0746 ± 0.0007	0.0225 ± 0.0010	0.0517 ± 0.0012	0.0140 ± 0.0006	0.0604 ± 0.0009
105	0.1746 ± 0.0003	1700 ± 100	0.0766 ± 0.0006	0.0224 ± 0.0009	0.0541 ± 0.0011	0.0138 ± 0.0006	0.0627 ± 0.0008
z = 8 mm				$\Delta\lambda_{VDW}$(nm) (supp 100 % vapour surr H)	$\Delta\lambda_{Stark}$(nm) (supp 100 % vapour in VDW)	$\Delta\lambda_{VDW}$(nm) (supposing 100 % He surr H)	$\Delta\lambda_{Stark}$(nm) (100 % He in VDW)
32	0.167 ± 0.007	1250 ± 100	0.065 ± 0.008	0.0278 ± 0.0016	0.037 ± 0.008	0.0172 ± 0.0010	0.048 ± 0.008
59	0.173 ± 0.005	1200 ± 100	0.076 ± 0.005	0.0287 ± 0.0017	0.047 ± 0.006	0.0177 ± 0.0010	0.058 ± 0.006
76	0.176 ± 0.007	1175 ± 100	0.079 ± 0.008	0.0291 ± 0.0017	0.050 ± 0.008	0.0180 ± 0.0011	0.061 ± 0.008
87	0.177 ± 0.003	1175 ± 100	0.081 ± 0.003	0.0291 ± 0.0017	0.052 ± 0.004	0.0180 ± 0.0011	0.063 ± 0.003
105	0.179 ± 0.003	1175 ± 100	0.083 ± 0.003	0.0291 ± 0.0017	0.054 ± 0.004	0.0180 ± 0.0011	0.065 ± 0.003

Fig. 9 shows the values of electron density measured for the discharges studied at axial positions z = 0 and 8 mm, corresponding to $\Delta\lambda_{Stark}$ values in Table III, considering a 100 % of helium, vapour and perturbers, respectively, in calculations.
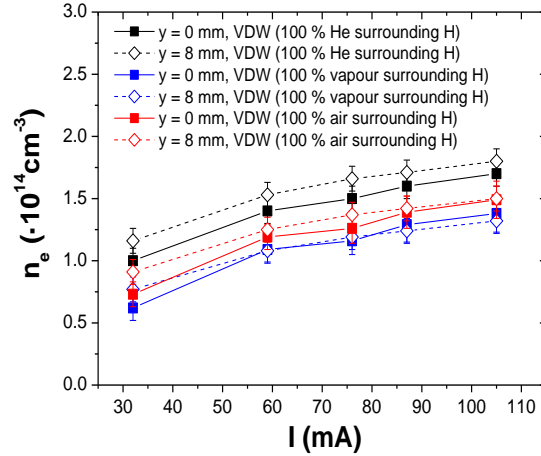
Figure 9. Electron density dependence on plasma current considering different pertubers surrounding H atom in the calculation of the van der Waals contribution.

Fig. 9 shows the values of electron density measured for the discharges studied at axial positions z = 0 and 8 mm, cor responding to λ_{Stark} values in Table III, considering a 100% of helium, vapor, and perturbers, respectively, in calculations. In any case, the plasma density grows almost linearly with increasing current. Also, as shown in Fig. 9, regardless of the variation in the compositions used in the van der Waals calculations, the calculated electron densities appear to be quite similar at the cathode region and at the liquid surface. This is quite remarkable as one expects region above the liquid to be liquid density owing to evaporation and thus more collisional with greater attachment losses. The similarities may be attributed to the presence of significant voltage drops in these regions (cathode and anode fall voltage/anode spot), which would drive ionization. At the surface, the high evaporation rate combined with the lower ionization potential of water (12.6 eV) may be enough to offset attachment and vibrational excitation losses, thereby slightly exceeding production in the cathode region as observed here. Intuitively, one can surmise that significant ionization takes place at the

surface as inferred from the bright, localized attachments at the water surface as well as the presence of helium emission. Excited helium near the surface can also contribute to Penning ionization. Assessing the magnitude of the electric field at the anode surface and in the cathode region is beyond the scope of this work and thus is left to future work.

D. Excitation temperature

The *excitation temperature* (T_{exc}) was estimated from the Boltzmann-plot representation [*log(Iλ/Ag)* versus E_p] obtained from H I lines measured (H$_\alpha$ and H$_\beta$). When the Saha ionization-recombination balance for the upper levels of H I system is established by electron collisions, the population of these levels conforms to a Saha-Boltzmann distribution with ionization and excitation temperatures equal to the electron temperature [39]. In the present case, it is not known whether or not this condition is fulfilled, so we only consider the excitation temperature obtained as a first estimation of electron temperature.
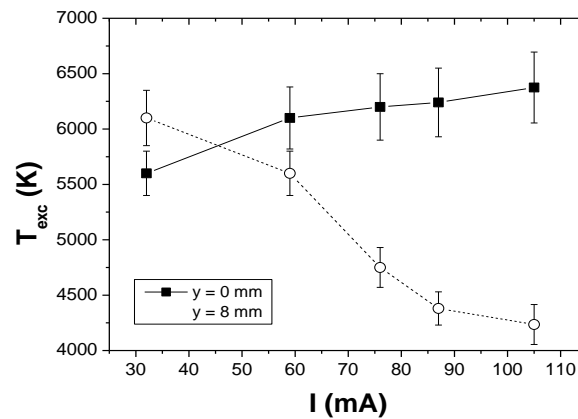

Figure 10. Excitation temperature dependence on plasma current

Fig. 10 shows the values of T_{exc} measured for positions y = 0 mm and y = 8 mm, where H I lines could be detected under all experimental conditions. As can be seen in the figure, the excitation temperature drops significantly near the liquid surface. This is

consistent with cooling effects owing to evaporation, the rate of which increases with increasing discharge power. This observation is consistent with the reduction in gas temperature with increasing voltage as well. The vapor has an overall cooling effect on the plasma near the anode. The excitation temperature near the cathode experiences slow growth with increasing input voltage.

E. Species emission

Next, a more detailed study of the emission of different excited species in the plasma is presented. Figs. 11 and 12(a) and (b) show the variations of the intensity of different emission lines observed in spectra, under different experimental conditions studied (error bars were not deliberately included in Fig. 12, in which different trends could be seen as clearly as possible).
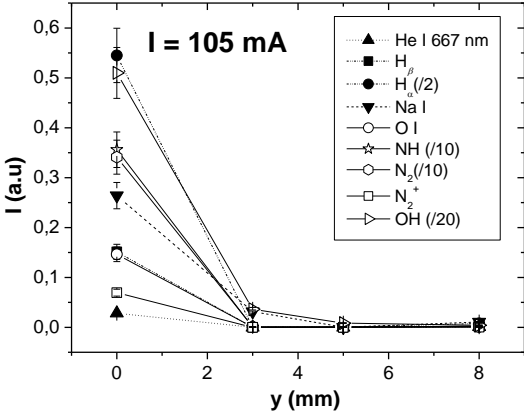
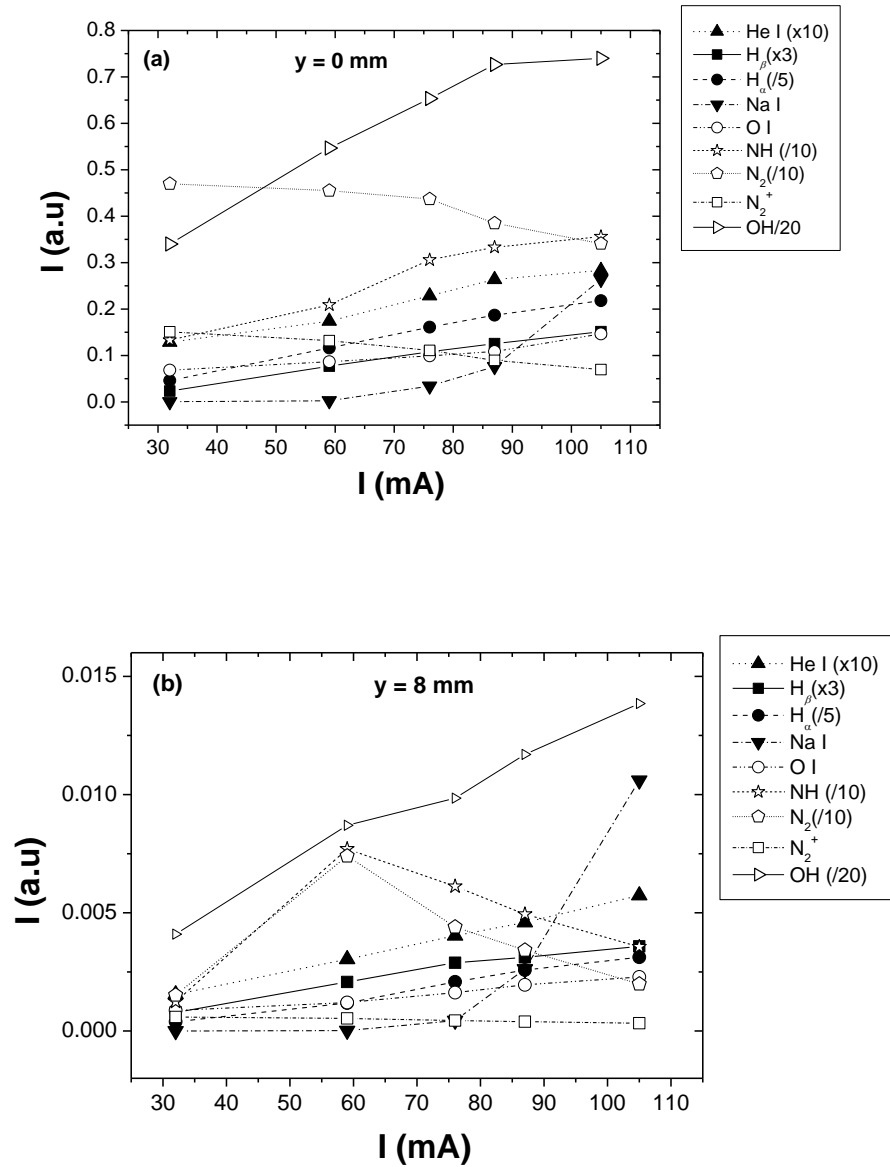**Figure 11.** Axial profile of the emission of different excited species in the plasma

Figure 12. Emission of the different excited species in the plasma near (a) the cathode and (b) the anode.

Helium was the carrier gas of the discharge, so likely helium excited atoms (including helium metastables atoms) could be playing an outstanding role in the kinetics of this plasma. Helium excited species 1s3d were observed mainly at the cathode region. The high excitation energy of these species (≈23 eV) explains their weak emission. Fig. 12(a) and (b) show the increase of the intensity of He I line with the

voltage (at positions y = 0 and y = 8 mm, respectively), in a similar trend as the electron density. In the spectra, excited hydrogen atoms and OH radicals were also detected, due to the presence of water vapor in the discharge.

The axial profiles of the emission of H_β and H_α hydrogen atomic lines (excitation energies 12.9 and 12.1 eV, respectively) were also plotted in Fig. 12(a) and (b). Fig. 12(a) and (b) show the increase of the intensity of hydrogen atomic lines emission with the discharge current, in a similar trend as electron density and helium lines intensity.

The emission of $OH(A^2\Sigma^+ \rightarrow X^2\Pi)$ rot-vibrational band was especially intense in the spectrum, which is partly due to the relatively low excitation energy of these states (≈ 4 eV). In Figures 11 and 12(a) and (b) the intensity of the band head of $OH(A^2\Sigma^+ \rightarrow X^2\Pi)$ band head measured in arbitrary units under the different experimental conditions studied is also included. This intensity decreased with increasing distance from the cathode, and increased with the current following the same trend as the intensity of He I and H I lines. The saturation observed for the 2.5 kV total voltage condition at position y = 0 mm could be ascribed to some self-absorption effects, enhanced by high amount of OH species existing in this case. It is also possible that electron temperature cooling owing to vapour injection may also play a role in the reduced excitation rate of this transition.

As a consequence of the entrance of air into the plasma, excited species containing nitrogen were also present in the spectra recorded. This fact is typical in discharges created in direct contact with the air. In this way, emission of the first negative system of molecular ion $N_2^+(B^2\Sigma_u^+ \rightarrow X^2\Sigma_g^+)$ (band head at at 391.44 nm) was detected. Helium metastables (19.8 eV) would have energy enough to create N_2^+(B) states (18.9 eV) from the following Penning type reactions like [40]

$$He^m + N_2(X^1\Sigma_g^+) \rightarrow He^0 + N_2^+(B^2\Sigma_u^+) + e^- \tag{7}$$
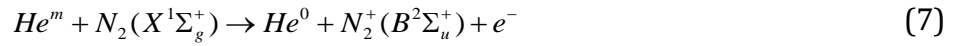
Dimer ions of nitrogen were mainly detected at a position near the cathode. The intensity of the band head of the first negative system of the molecular ion N_2^+ followed a different behavior with voltage when compared to those of helium and hydrogen atoms and OH radicals. An inferred decrease in the amount of species N_2^+ (B) was observed when the voltage applied (and the discharge current) was raised, even though the amount of helium species increased. This fact should be probably due to the higher concentration of water vapor (and reduction of the fraction of air present) in the discharge, quenching activated helium species.

Nitrogen molecules were also detected. Excited helium neutrals have more than enough energy to excite any state of the N_2 second positive system (excitation energy $\approx$ 11. 1 eV). As in the case of N_2^+ emission, the intensity of the N_2 ($C^3\Pi_u \rightarrow B^3\Pi_g$) band head at 337.13 nm the change with the voltage did not follow the same trend as electron density.

As already mentioned, the presence of NH species was also identified from OES (see Figs. 12). This diatomic association molecule could be generated by

$$N + H_2O \rightarrow NH + OH \tag{8}$$

Dissociative recombination reactions are considered as a possible channel for molecular nitrogen ions destruction and *N* formation in plasmas open to the air generated at atmospheric pressure [41]

$$N_2^+ + e^- \rightarrow N + N \tag{9}$$

This reasoning could explain the reduction of the amount of species N_2^+ observed at y = 0 mm position when the current increased, taking place at the same time as the amount of species NH and OH increases.

The presence of excited oxygen atomic species in these discharges was also indicative of the inlet of air into them. Optical emission at 777.2 nm, corresponding to transitions from *3p* states ($\approx 10.7\text{eV}$) of O I system, was observed. These species were probably created by dissociative recombination of O_2^+ species generated from Penning-type reactions

$$He^m + O_2(X^3\Sigma_g^-) \rightarrow He^0 + O_2^+(b^4\Sigma_g^-) + e^- \tag{10}$$
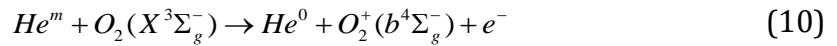
The population of O I species also increased with voltage (see Fig. 12).

Finally, the emission of Na I 589.59 nm line is shown in Fig. 12. In this case, an exponential increase of the emission with the voltage was observed consistently with increased evaporation rate with input power.

IV. Conclusion

OES was used to assess the plasma conditions of a dc 1-atm glow discharge. This work found that the discharge species composition depends on spatial location. This work also highlights the importance of localized boiling. This data suggest that the introduction of the associated water vapor plays a role in cooling the plasma locally. In addition, the droplet entrainment by steam is apparently a vehicle for the introduction of solute into the gas phase as well, such as metal ions including sodium and iron observed here. Interesting chemistry was observed in the cathode region with the production of NH radicals. These radicals could potentially serve as precursors for the production of ammonia. The observed helium emission near the cathode and liquid anode suggests nontrivial anode and cathode fall voltages, which apparently serves to accelerate electrons to energies necessary to excite the helium. This observation may be the underlying reason for the relative similarities between the electron density near the cathode and that near the liquid anode. Finally, the overall shape of the sodium vapor cloud appears to be consistent with what one would expect of localized boiling. Here, the

localized anode attachment is the heat source for evaporation with vapor leaving in the expected cosine distribution.

Acknowledgements

References

[1] G. Nicolis and I. Prigogine, "Self-organisation in nonequilibrium systems: Towards a dynamics of complexity," in Bifurcation Analysis, M. Hazewinkel, R. Jurkovich, and J. H. P. Paelinck, Eds., 1st ed. Dordrecht, The Netherlands: D. Reidel Publishing Company, 1985, pp. 3–12.

[2] O. Lehmann, "Gasentladungen in weiten Gefässen," Annalen Physik, vol. 312, no. 1, pp. 1–28, 1902.

[3] C. Radehaus, T. Dirksmeyer, H. Willebrand and H.-G. Purwins, "Pattern formation in gas discharge systems with high impedance electrodes," Phys. Lett. A, vol. 125, no. 2, pp. 92–94, Nov. 1987.

[4] Y. A. Astrov and H.-G. Purwins, "Plasma spots in a gas discharge system: Birth, scattering and formation of molecules," Phys. Lett. A, vol. 283, no. 5, pp. 349–354, 2001.

[5] R. S. Islamov, "Physical model of anode glow patterns in elevatedpressure gas discharges," Phys. Rev. E, Stat. Phys. Plasmas Fluids Relat. Interdiscip. Top., vol. 64, no. 4, Sep. 2001, Art. no. 046405.

[6] M. Sanduloviciu, E. Lozneanu, and S. Popescu, "On the physical basis of pattern formation in nonlinear systems," Chaos, Solitons Fractals, vol. 17, no. 2, pp. 183–188, 2003.

[7] M. S. Benilov, "Bifurcations of current transfer through a collisional sheath with ionization and self-organization on glow cathodes," Phys. Rev. E, Stat. Phys. Plasmas Fluids Relat. Interdiscip. Top., vol. 77, no. 3, Mar. 2008, Art. no. 036408.

[8] K. G. Müller, "Structures at the electrodes of gas discharges," Phys. Rev. A, Gen. Phys., vol. 37, no. 12, pp. 4836–4845, Jun. 1988.

[9] Y. P. Raizer and M. S. Mokrov, "Physical mechanisms of selforganization and formation of current patterns in gas discharges of the Townsend and glow types," Phys. Plasmas, vol. 20, no. 10, Oct. 2013, Art. no. 101604.

[10] A. A. Berezin, "Electrostatic stability and instability of N equal charges in a circle," Chem. Phys. Lett., vol. 123, no. 1, pp. 62–64, Jan. 1986.

[11] J. P. Trelles, "Formation of self-organized anode patterns in arc discharge simulations," Plasma Sources Sci. Technol., vol. 22, no. 2, Mar. 2013, Art. no. 025017.

[12] M. S. Bieniek, P. G. C. Almeida, and M. S. Benilov, "Self-consistent modeling of self-organized patterns of spots on anodes of DC glow discharges," Plasma Sources Sci. Technol., vol. 27, no. 5, May 2018, Art. no. 05LT03.

[13] P. Bruggeman et al., "Plasma-liquid interactions: A review and roadmap," Plasma Sources Sci. Technol., vol. 25, no. 5, Sep. 2016, Art. no. 053002.

[14] T. Verreycken, P. Bruggeman, and C. Leys, "Anode pattern formation in atmospheric pressure air glow discharges with water anode," J. Appl. Phys., vol. 105, no. 8, pp. 083312-1–083312-4, 2009.

[15] A. Wilson, D. Staack, T. Farouk, A. Gutsol, A. Fridman, and B. Farouk, "Self-rotating DC atmospheric-pressure discharge over a water-surface electrode: Regimes of operation," Plasma Sources Sci. Technol., vol. 17, no. 4, 2008, Art. no. 045001.

[16] P. Bruggeman, J. Liu, J. Degroote, M. G. Kong, J. Vierendeels, and C. Leys, "DC excited glow discharges in atmospheric pressure air in pinto-water electrode systems," J. Phys. D: Appl. Phys., vol. 41, Oct. 2008, Art. no. 215201.

[17] N. Shirai, S. Uchida, and F. Tochikubo, "Influence of oxygen gas on characteristics of self-organized luminous pattern formation observed in an atmospheric DC glow discharge using a liquid electrode," Plasma Sources Sci. Technol., vol. 23, no. 5, Sep. 2014, Art. no. 054010.

[18] N. Shirai, S. Ibuka, and S. Ishii, "Self-organization pattern in the anode spot of an atmospheric glow microdischarge using an electrolyte anode and axial miniature helium flow," Appl. Phys. Express, vol. 2, no. 3, Mar. 2009, Art. no. 036001.

[19] N. Shirai, S. Uchida, F. Tochikubo, and S. Ishii, "Self-organized anode pattern on surface of liquid or metal anode in atmospheric DC glow discharges," IEEE Trans. Plasma Sci., vol. 39, no. 11, pp. 2652–2653, Nov. 2011.

[20] S. Y. Miao, C. S. Ren, D. Z. Wang, Y. T. Zhang, B. Qi, and Y. N. Wang, "Conical DC discharge in ambient air using water as an electrode," IEEE Trans. Plasma Sci., vol. 36, no. 1, pp. 126–130, Feb. 2008.

[21] M. J. Aschwanden et al., "Order out of randomness: Self-organization processes in astrophysics," Space Sci. Rev., vol. 214, no. 2, p. 55, Mar. 2018.

[22] A. De Wit, "Spatial patterns and spatiotemporal dynamics in chemical systems," in Advances in Chemical Physics, vol. 109, I. Prigogine and S. A. Rice, Eds. Ottawa, ON, Canada: Wiley, 1999, pp. 435–513. [Online]. Available: https://onlinelibrary.wiley.com

[23] K. Showalter and I. R. Epstein, "From chemical systems to systems chemistry: Patterns in space and time," Chaos, vol. 25, no. 9, Apr. 2015, Art. no. 097613.

[24] N. Shirai, S. Uchida, and F. Tochikubo, "Synthesis of metal nanoparticles by dual plasma electrolysis using atmospheric DC glow discharge in contact with liquid," Jpn. J. Appl. Phys, vol. 53, no. 4, 2014, Art. no. 046202.

[25] R. K. Bagul, D. S. Pilkhwal, P. K. Vijayan, and J. B. Joshi, "Entrainment phenomenon in gas–liquid two-phase flow: A review," Sadhana, vol. 38, no. 6, pp. 1173–1217, 2013.

[26] R. F. Davis, "The physical aspect of steam generation at high pressures and the problem of steam contamination," Proc. Inst. Mech. Eng., vol. 144, no. 1, pp. 198–216, Jun. 1940.

[27] N. Shirai, M. Nakazawa, S. Ibuka, and S. Ishii, "Atmospheric DC glow microplasmas using miniature gas flow and electrolyte cathode," Jpn. J. Appl. Phys., vol. 48, no. 3, Mar. 2009, Art. no. 036002.

[28] N. Shirai, T. Yoshida, S. Uchida, and F. Tochikubo, "Synthesis of magnetic nanoparticles by atmospheric-pressure glow discharge plasmaassisted electrolysis," Jpn. J. Appl. Phys., vol. 56, no. 7, Jun. 2017, Art. no. 076201.

[29] M. Knudsen, "The cosine law in the kinetic theory of gases, translation of das cosinusgesetz in der kinetischen gastheorie," Annalender Physik, vol. 48, no. 4, pp. 1113–1121, 1915.

[30] A. Powell, P. Minson, G. Trapaga, and U. Pal, "Mathematical modeling of vapor-plume focusing in electron-beam evaporation," Metall. Mater. Trans. A, vol. 32, no. 8, pp. 1959–1966, Aug. 2001.

[31] J. H. van Helden, P. J. van den Oever, W. M. M. Kessels, M. C. M. van de Sanden, D. C. Schram, and R. Engeln, "Production mechanisms of NH and NH2 radicals in N2-H2 plasmas," J. Phys. Chem. A, vol. 111, no. 45, pp. 11460–11472, Oct. 2007.

[32] A. V. Bernatskiy, V. N. Ochkin, and I. V. Kochetov, "Multispectral actinometry of water and water-derivative molecules in moist, inert gas discharge plasmas," J. Phys. D: Appl. Phys., vol. 49, no. 39, Sep. 2016, Art. no. 395204.

[33] J. Luque and D. R. Crosley, "LIFBASE: Database and spectral simulation program," SRI Int., Menlo Park, CA, USA, Tech. Rep. MP 99-009, Version 1.9, 1999.

[34] A. Y. Nikiforov, C. Leys, M. A. Gonzalez, and J. L. Walsh, "Electron density measurement in atmospheric pressure plasma jets: Stark broadening of hydrogenated and non-hydrogenated lines," Plasma Sources Sci. Technol., vol. 24, no. 3, Apr. 2015, Art. no. 034001.

[35] A. Rodero and M. C. Garcia, "Gas temperature determination of nonthermal atmospheric plasmas from the collisional broadening of argon atomic emission lines," J. Quant. Spectrosc. Radiat. Transf., vol. 198, pp. 93–103, Sep. 2017.

[36] C. O. Laux, T. G. Spence, C. H. Kruger, and R. N. Zare, "Optical diagnostics of atmospheric pressure air plasmas," Plasma Sources Sci. Technol., vol. 12, no. 2, pp. 125–138, May 2003.

[37] P. Bruggeman, D. Schram, M. Á. González, R. Rego, M. G. Kong, and C. Leys, "Characterization of a direct DC-excited discharge in water by optical emission spectroscopy," Plasma Sources Sci. Technol., vol. 18, no. 2, Mar. 2009, Art. no. 025017.

[38] C. Yubero, M. D. Calzada, and M. C. Garcia, "Using the stark broadening of the Hα, Hβ and HY lines for the measurement of electron density and temperature in a plasma at atmospheric pressure," J. Phys. Soc. Jpn., vol. 74, no. 8, pp. 2249–2254, Aug. 2005.

[39] J. A. M. van der Mullen, "Excitation equilibria in plasmas; a classification," Phys. Rep., vol. 191, no. 2, pp. 109–220, 1990.

[40] Q. S. Yu and H. K. Yasuda, "An optical emission study on expanding low-temperature cascade arc plasmas," Plasma Chem. Plasma Process., vol. 18, no. 4, pp. 461–485, Dec. 1998.

[41] E. A. H. Timmermans et al., "The behavior of molecules in microwaveinduced plasmas studied by optical emission spectroscopy. 1. Plasmas at atmospheric pressure," Spectrochim. Acta B, At. Spectrosc., vol. 53, no. 11, pp. 1553–1566, 1998.